SCIENTIFIC REP⬤RTS

# NMR studies on the interactions between yeast Vta1 and Did2 during the multivesicular bodies sorting pathway

Jie Shen[1,2,*], Zhongzheng Yang[1,3,*], Jiaolong Wang[1], Bin Zhao[1], Wenxian Lan[1], Chunxi Wang[1], Xu Zhang[4], Cody J. Wild[5], Maili Liu[4], Zhaohui Xu[5] & Chunyang Cao[1]

As an AAA-ATPase, Vps4 is important for function of multivesicular bodies (MVB) sorting pathway, which involves in cellular phenomena ranging from receptor down-regulation to viral budding to cytokinesis. The activity of Vps4 is stimulated by the interactions between Vta1 N-terminus (named as Vta1NTD) and Did2 fragment (176–204 aa) (termed as $Did2_{176-204}$) or Vps60 (128–186 aa) (termed as $Vps60_{128-186}$). The structural basis of how Vta1NTD binds to $Did2_{176-204}$ is still unclear. To address this, in this report, the structure of $Did2_{176-204}$ in complex with Vta1NTD was determined by NMR techniques, demonstrating that $Did2_{176-204}$ interacts with Vta1NTD through its helix $\alpha6'$ extending over the 2nd and the 3rd α-helices of Vta1NTD microtubule interacting and transport 1 (MIT1) domain. The residues within $Did2_{176-204}$ helix $\alpha6'$ in the interface make up of an amino acid sequence as $E_{192}'xxL_{195}'xxR_{198}'L_{199}'xxL_{202}'R_{203}'$, identical to type 1 MIT-interacting motif (MIM1) (D/E) xxLxxRLxxL(K/R) of $CHMP1A_{180-196}$ observed in Vps4-CHMP1A complex structure, indicating that Did2 binds to Vta1NTD through canonical MIM1 interactions. Moreover, the Did2 binding does not result in Vta1NTD significant conformational changes, revealing that Did2, similar to Vps60, enhances Vta1 stimulation of Vps4 ATPase activity in an indirect manner.

The ESCRT (endosomal sorting complexes required for transport) machinery[1–3], initially identified in the yeast multivesicular bodies (MVBs) biogenesis pathway[3,4], protects against age-related neurodegenerative diseases through either the canonical MVB pathway[5–7] or autophagy[8,9], and plays a pathological role in viral infection[6,10,11]. It is made up of ESCRT-0, ESCRT-I, ESCRT-II, ESCRT-III and Vps4 complexes[12,13]. ESCRT-0 is responsible for clustering of ubiquitylated cargoes to the site of MVB formation. ESCRT-I and ESCRT-II together generate membrane curvature and bud while assembly of ESCRT-III at the bud neck catalyzes the scission of membrane. These components have been identified as potential tumor suppressors[8], mainly due to the involvement of the ESCRT machinery in regulating signal attenuation for activated receptors of growth factors, peptide hormones and cytokines. Vps4 is an AAA-ATPase, which disassembles ESCRT-III polymers upon ATP binding and hydrolysis[14,15].

The biogenesis of lysosomes involves the maturation of early endosomes into MVBs. During this pathway, portions of limiting membrane of the endosome invaginate and then detach into lumen of endosome, forming intraluminal vesicles (ILVs)[6,7]. Then MVBs fuse with the lysosome and ILVs, thus their components are degraded. The cell surface receptors for down-regulation and some enzymes located in lysosomes are sorted

[1]State Key Laboratory of Bioorganic and Natural Products Chemistry and Collaborative Innovation Center of Chemistry for Life Sciences, Shanghai Institute of Organic Chemistry, Chinese Academy of Sciences, 345 Lingling Road, Shanghai, 200032, China. [2]Tianjin Institute of Industrial Biotechnology, Chinese Academy of Sciences, 32 XiQiDao, Tianjin Airport Economic Area, Tianjin, 300308, China. [3]Public Technology Service Platform, Wuhan Institute of Biotechnology, 666 Gaoxin Road, Wuhan, 430075, China. [4]State Key Laboratory of Magnetic Resonance and Atomic and Molecular Physics, Wuhan Institute of Physics and Mathematics, Chinese Academy of Sciences, 30 West Xiaohongshan Road, Wuhan, 430071, China. [5]Life Sciences Institute and Department of Biological Chemistry, Medical School, University of Michigan, 210 Washtenaw Ave, Ann Arbor, MI 48109, USA. *These authors contributed equally to this work. Correspondence and requests for materials should be addressed to C.C. (email: ccao@mail. sioc.ac.cn)
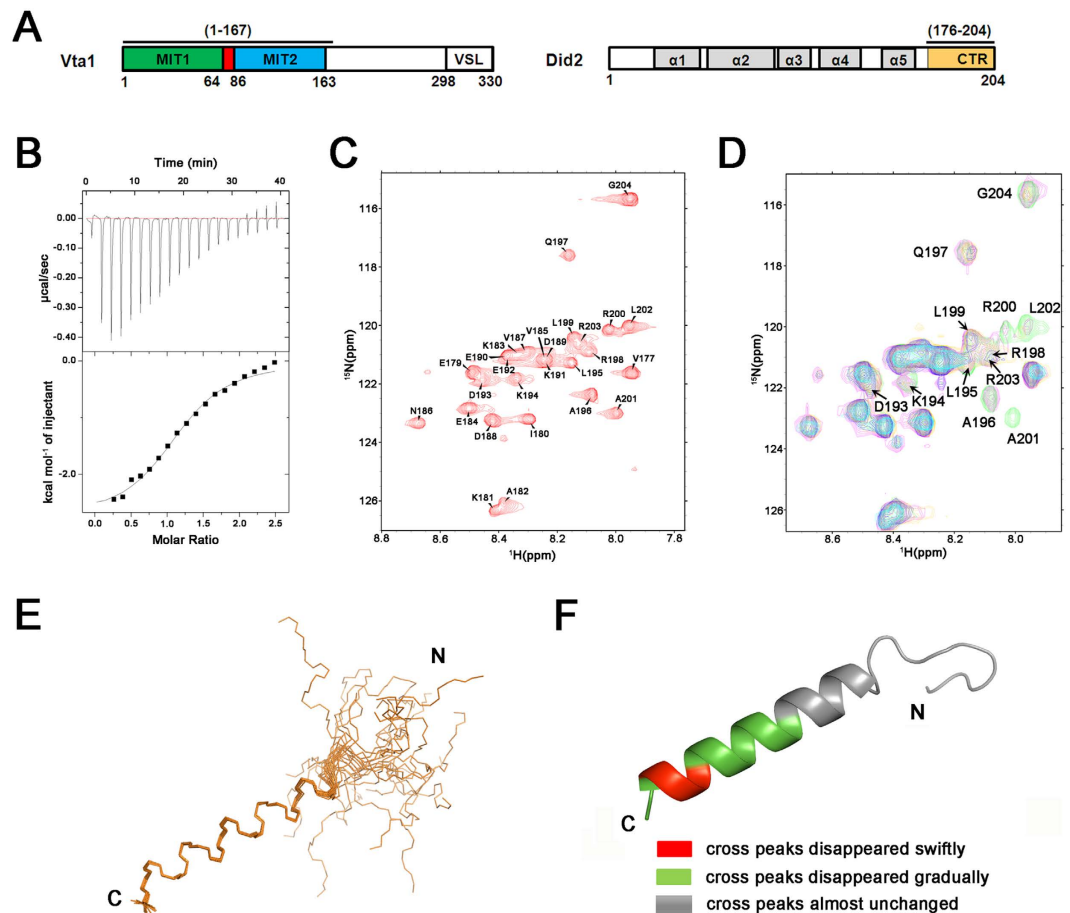
Figure 1. Did2₁₇₆₋₂₀₄ MIM interacts withVta1NTD. (**A**) Schematic representation of Vta1 and Did2, highlighting regions critical for interactions that contribute to increased Vps4 ATPase activity. (**B**) The binding affinity of Did2$_{176-204}$ to Vta1NTD, measured by ITC assay. Upper panel shows the raw data for the titration of Did2$_{176-204}$ with Vta1NTD and lower panel displays the heats of binding integrated from the peaks. The solid line in the bottom panel represent the best curve fit to the experimental data. (**C**) NMR signal assignments of the cross-peaks in the ¹H-¹⁵N HSQC spectrum of free Did2$_{176-204}$. (**D**) NMR titration of Vta1NTD into Did2$_{176-204}$ at mole ratios (Did2$_{176-204}$ *vs* Vta1NTD) of 1:0 (green), 1:0.1 (red), 1:0.2 (golden), 1:0.4 (blue), 1:1.2 (cyan). The residues D193-G204, corresponding to the residues marked in red and green in Fig. 1F, whose cross peaks finally disappeared during titration, were highlighted. (**E**) The backbone view of the ensemble of 20 lowest-energy free Did2$_{176-204}$ structures. (**F**) Ribbon representation of free Did2$_{176-204}$, the residues whose cross-peaks disappeared swiftly, disappeared gradually and almost unchanged were highlighted in red, green and grey colors, respectively.

into this endo-lysosomal degradation pathway[16]. The ATP consuming reaction is the only step in MVB biogenesis that inputs energy to the system, therefore providing the thermodynamic driving force for disassembly process. The function of Vps4 is conserved in all biological processes that depend on the action of the ESCRTs. Identical to other AAA-ATPases, Vps4 acts as an oligomer with two conformationally distinctive hexameric rings[17]. These two rings have a central pore, so that ESCRT-III subunits may physically interact Vps4 and pass through this pore during the disassembly process. Vps4 interacts with ESCRT-III subunits through its N-terminal microtubule-interacting and transport (MIT) domain[18], which appears to specifically identify short peptide sequence MIT-interacting motifs (MIMs) at or near the C-terminal end of ESCRT-III subunits[19–24].

Vta1, Did2, Ist1 and Vps60 are ESCRT-III related proteins, which have been identified to bind to Vps4 and play key roles in regulating the oligomerization and activity of Vps4 *in vivo*[25–29]. Vta1 is a positive regulator of Vps4 by promoting Vps4 oligomerization[26,30]. Based on its structural studies, Vta1 is a molecular dimer with each subunit folded into two terminal domains linked by a flexible linker[29]. Its C-terminal domain mediates dimerization and binds to a unique β-domain in the Vps4 AAA domain[31,32]. Its N-terminal domain (residues 1–167 and was named as Vta1NTD in this report, Fig. 1A) contains two tandem MIT domains, which specifically recognize Vps60 and Did2[27,29]. The fragment Vps60 (128–186aa) (termed as Vps60$_{128-186}$) was reported to display full activity of Vps60, which stimulates Vps4 ATPase in a Vta1-dependent manner[27]. Our NMR structural studies on the interactions between Vta1NTD and Vps60$_{128-186}$ revealed that Vps60$_{128-186}$ interacted with Vta1NTD in a novel MIT recognition mode, *i.e.*, through its helices α4′ and α5′ extending over helices 5, 6 and 7 of Vta1NTD MIT2 domain[33–36]. Previous studies indicated that the C-terminal of Did2, residues 176–204, named as Did2$_{176-204}$ in this whole

report, as shown in Fig. 1A, could enhance Vps4 ATPase activities as the full-length Did2[27,29]. In this report, to investigate how Did2 interacted with Vta1NTD, we first measured the binding affinity of Vta1NTD to Did2$_{176–204}$ by isothermal titration calorimetry (ITC) assay ($K_D = 12.8 \pm 1.0 \mu M$, the number N = 1.16 ± 0.0266) (Fig. 1B), and then determined the solution structure of Vta1NTD in complex with Did2$_{176–204}$. This structure revealed that Did2$_{176–204}$ bound to Vta1NTD through canonical type 1 MIT-interacting motif (MIM1) interactions.

Results and Discussion

The suggested MIM region of Did2$_{176–204}$ forms an α-helix conformation. Secondary structure prediction and perceived structural homology to ESCRT-III protein Vps24/CHMP3 suggest that Did2$_{176–204}$ corresponds to the 6th helix within the Did2 structure[37]. This helix conformation was confirmed by our following NMR studies. We first assigned its NMR signals based on two-dimensional (2D) ^{1}H-^{1}H TOCSY and NOESY, three-dimensional (3D) ^{15}N-edited HSQC-TOCSY spectra. In its 2D NMR ^{1}H-^{15}N HSQC experiment (Fig. 1C), the cross peaks belonging to 27 residues were assigned, except the N-terminal residues N$_{176}$ and P$_{178}$ (without amide proton). We then determined its NMR solution structure using 191 distance restraints from NOE and 26 hydrogen bonds. Finally, 20 structures with the lowest-energy could be well fitted (Fig. 1E) with the RMSD values of 0.15 ± 0.06 Å for the backbone atoms, and of 0.88 ± 0.09 Å for all heavy atoms in secondary structure region. The Ramachandran plot displays 93.1% of the residues in the most-favored regions, 4.0% residues in additionally allowed regions, and 2.9% residues in generously allowed regions, indicating that the structures are acceptable. The solution structures demonstrate that the region of Did2 187–204 aa forms an α-helix, consistent with the observation in the crystal structure of complex Did2-Ist1[27,29].

To study how Vta1NTD interacts with Did2$_{176–204}$, we performed NMR titration experiments, in which Vta1NTD was titrated into Did2$_{176–204}$ at mole ratios (Vta1NTD *vs* Did2$_{176–204}$) of 0.1:1, 0.2:1, 0.4:1, 0.6:1, 0.8:1 and 1.2:1 in NMR buffer conditions. The cross peaks belonging to residues R$_{200}$A$_{201}$L$_{202}$ disappeared even at mole ratios of 0.1:1 and 0.2:1, while the cross peaks belonging to D193-L199 and R$_{203}$G$_{204}$ became weaker and weaker upon the concentration of Vta1NTD being increased. At the mole ratio of 1.2:1, the cross peaks belonging to residues V177-E192 almost unchanged (Fig. 1D). These observations suggest that the residues D193-G204 are involved in the interactions, and that the MIM sequence of Did2$_{176–204}$ bind to Vta1NTD. This hypothesis was consistent with our observation in the complex structure (discussed below), where the residues in the region of 187–204aa interact with Vta1NTD MIT1 domain.

NMR structural determination of complex Vta1NTD-Did2$_{176–204}$. Using two basic sets of NMR samples: 1) ^{13}C and ^{15}N isotope double labeled or ^{13}C, ^{15}N and 70% ^{2}H triple-labeled Vta1NTD mixed with unlabeled Did2$_{176–204}$ at the stoichiometric ratio of 1:1.2, 2) ^{13}C and ^{15}N isotope labeled Did2$_{176–204}$ mixed with unlabeled Vta1NTD at stoichiometric ratio of 1:1.2, and by running a series of 2D and 3D NMR experiments, in total, more than 94% NMR signals of the main-chain and 95% NMR signals of the side-chain atoms of the residues in the complex were assigned. The inter-molecule NOEs were correctly assigned by confirming signals observed in 3D ^{13}C-F1 edited, ^{13}C/^{15}N-F3 filtered NOESY spectra acquired on both complex samples. The NMR chemical shift changes of Vta1NTD backbone atoms ^{1}H and ^{15}N in the absence of and in the presence of Did2$_{176–204}$ reveal that Did2$_{176–204}$ addition mainly induces amide ^{15}N and ^{1}H chemical shifts variation of the residues in Vta1NTD MIT1 (Fig. 2A), suggesting that Did2$_{176–204}$ binding sites locate in this region. This observation accords with the previous analysis on chemical shift mapping of CHIMP1B-binding site on LIP5(MIT)$_2$[35], and with the analysis of electrostatic surface of Vta1NTD, which shows that Vta1NTD MIT1 is more negatively charged and more hydrophobic than its MIT2 (Fig. 2B), suitable for positively charged and hydrophobic Did2$_{176–204}$ binding.

The solution structure of Vta1NTD-Did2$_{176–204}$ complex was then determined by a conventional heteronuclear NMR method using ^{15}N-labeled or ^{13}C/^{15}N-labeled proteins. In total, 2730 distance restraints from NOE (including 36 inter-molecular NOEs), 236 hydrogen bonds and 676 dihedral angle restraints for backbone φ and ψ angles were used to calculate solution structure. The best-fit superposition of the ensemble of the 20 lowest-energy structures represented in Fig. 2C was displayed with the RMSD values of 0.82 ± 0.17 Å for the backbone (N, C$_\alpha$ and CO) atoms and 1.14 ± 0.15 Å for all heavy atoms in the well-ordered second structure regions. The Ramachandran plot displays 97.8% of the residues in the most-favored regions and 2.1% residues in additionally allowed regions (Table 1), indicating the structures are reasonable.

Overall complex structure. The complex Vta1NTD-Did2$_{176–204}$ structure shows that the bound Vta1NTD still has two MIT domains, each of them is composed of three α-helices (MIT1: helices α1, α2 and α3; MIT2: helices α5, α6 and α7; respectively), almost similar to those observed in its free state and in its complex with Vps60$_{128–186}$[29,33–36]. The backbone atoms belonging to MIT1 and MIT2 regions of bound Vta1NTD have RMSD values of 1.7 Å and 1.8 Å with those of free Vta1NTD (Fig. 2D), respectively, indicating that Did2$_{176–204}$ binding does not induce overall major conformational changes in Vta1NTD. The linker (64–85aa) between MIT1 and MIT2 domains is well ordered, where residues 66–69 become an α-helix, and residues 73–84 adopt a longer helical structure (here we called it as helix α4) (Fig. 2E)[33,34]. The helix α4 is much longer in Vta1NTD-Did2$_{176–204}$ than that in free Vta1NTD crystal structure, but similar to the observation in NMR structure of Vta1NTD bound to Vps60$_{128–186}$[33–35]. This observation is consistent with our previous secondary structure prediction of free Vta1NTD using the programs CSI[38] and TALOS[39,40] based on the assignments of NMR signals belonging to the backbone atoms of Vta1NTD. In contrast, this linker in free Vta1NTD crystal structure adopts largely random-coil structure with only a one-turn α-helix occurring at residues 80–84. Particularly, residues 65–75 appear to be disordered in the structure of free Vta1NTD. Thus, this conformational change might be caused by the interactions between helix α4 (73–84) of Vta1NTD and Vps60$_{128–186}$ or Did2$_{176–204}$, or by stacking during free Vta1NTD crystallization.
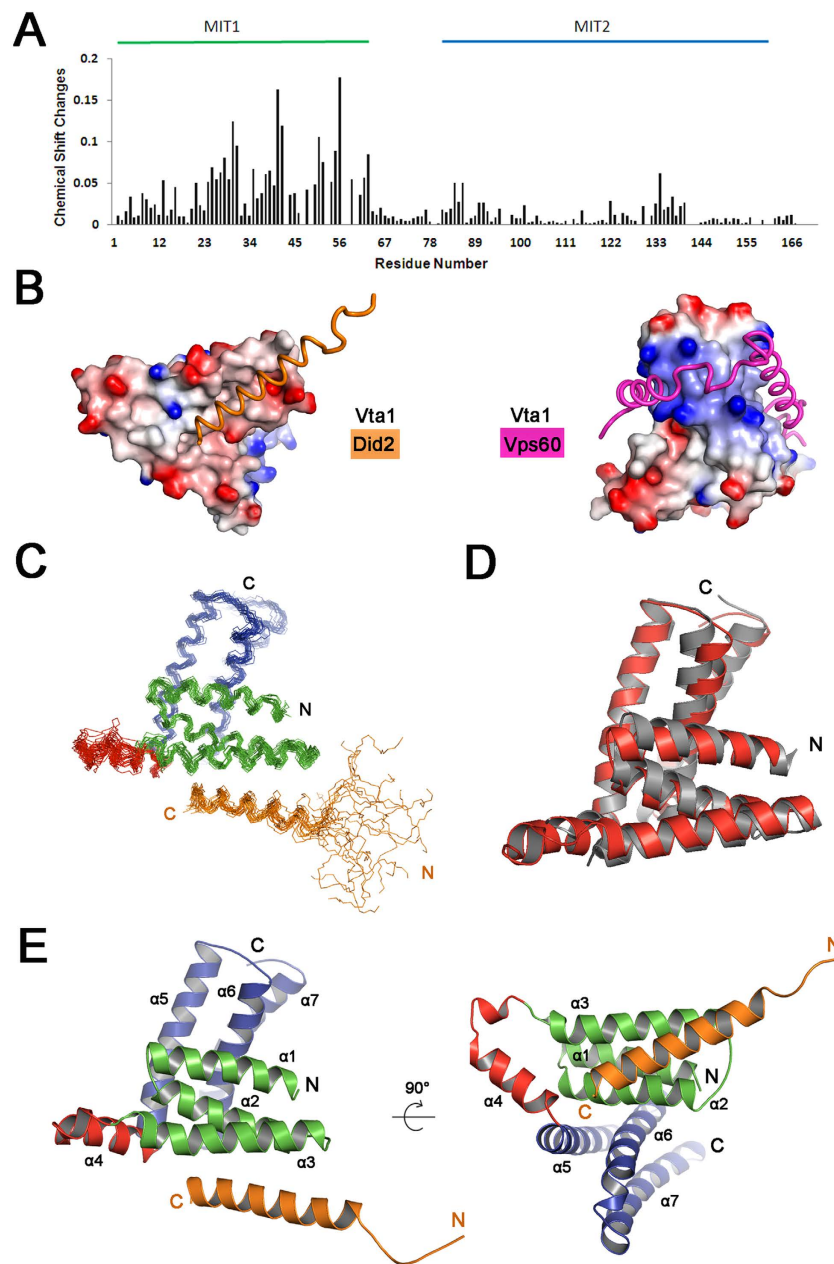
Figure 2. Did2$_{176-204}$ interacts with helices 2/3 of Vta1NTD MIT1 motif. (**A**) The Chemical shift changes of Vta1NTD backbone atoms amide ^{1}H and ^{15}N upon Did2$_{176-204}$ binding, calculated by using the equation: $\Delta S_{av} = \{0.5 \times [\Delta\delta(NH)^2 + (0.2 \times \Delta\delta(N))^2]\}^{1/2}$. The MIT1 and MIT2 domains are indicated at the top based on the crystal structure of free Vta1NTD (PDB ID: 2RKK). (**B**) Differences in electrostatic potential surfaces between MIT1 and MIT2 of Vta1NTD. The electrostatic potential surface was generated based on the crystal structure of free Vta1NTD by using software DelPhi and visualized by PyMol. The Did2 and Vps60 were displayed in orange and pink tube mode, respectively. (**C**) Backbone view of the ensemble of 20 lowest-energy Vta1NTD-Did2$_{176-204}$ NMR structures, where Did2$_{176-204}$ is displayed in orange. (**D**) Structural overlay of free Vta1NTD (grey) (pdb code 2RKK) and bound Vta1NTD to Did2$_{176-204}$ (red). The N and C termini and the secondary structures are indicated. (**E**) 3D representative structure of Vta1NTD-Did2$_{176-204}$. The helices are numbered. In (**C**) and (**E**), the MIT1 and MIT2 domains of Vta1NTD, the linker between MIT1 and MIT2, and Did2$_{176-204}$ were displayed in blue, green, red and orange colors, respectively.

Within our expectation, in the current complex structure, the Did2$_{176-204}$ folds into one α-helix (denoted as α6′ helix hereafter), which is involved in the interaction with the first MIT domain of Vta1NTD (Fig. 2E). The bound Did2$_{176-204}$ adopts an overall rod-like helix structure with a flexible loop in its N-terminus (similar to free Did2$_{176-204}$ with an RMSD value of 0.5 Å for the backbone atoms in secondary structure region). The helix consists of residues 187′–203′, a little longer than that (residues 184′–198′) observed in LIP5NTD-CHIMP1B

Experimental restraints and structural statistics		
NMR distance and Dihedral Constraints	Vta1NTD-Did2$_{176-204}$	free Did2$_{176-204}$
Distance restraints from NOEs		
Intra-molecular		
Total	1811	191
Intra-residue (i-j = 0)	778	102
Sequential (|i-j| = 1)	487	78
Medium range (1<|i-j|≤5)	434	11
Long range (|i-j|>5)	112	0
Inter-molecular	36	
Hydrogen bonds	236	26
Dihedral restraints	390	
φ	195	
ψ	195	
Structural statistics[a]		
R.m.s Deviations versus the mean structure (Å)		
All backbone atoms	2.29 ± 0.53	3.14 ± 0.90
All heavy atoms	2.52 ± 0.49	3.71 ± 0.83
Backbone atoms (secondary structure)	0.82 ± 0.17	0.15 ± 0.06
Heavy atoms (secondary structure)	1.14 ± 0.15	0.88 ± 0.09
R.m.s. deviations from the experimental restraints		
NOE distances (Å)	0.034 ± 0.0007	0.24 ± 0.008
Dihedral angles (°)	0.53 ± 0.032	
R.m.s. deviations from idealized geometry		
Bonds (Å)	0.002 ± 0.00003	1.56 ± 0.00009
Angles (°)	0.28 ± 0.0068	0.25 ± 0.012
Impropers (°)	0.27 ± 0.006	0.21 ± 0.009
Ramachandran analysis		
Residues in most favored regions	97.8%	93.1%
Residues in additionally allowed regions	2.1%	4.0%
Residues in generously allowed regions	0.1%	2.0%
Residues in disallowed regions	0.0%	0.0%

Table 1. Experimental restraints and structural statistics for Vta1NTD-Did2$_{176-204}$ complex and free Did2$_{176-204}$. [a]Structural statistics was calculated from 20 lowest-energy XPLOR-NIH structure.

complex structure[36]. The Did2$_{176-204}$ α-helix sits on the surface groove formed by the 2nd and the 3rd helices of Vta1NTD MIT1 in a mode similar to that observed in Vps4-CHMP1A complex structure[20] and that observed in human LIP5NTD-CHMP1B and LIP5NTD-CHMP1B-CHMP5 complex structures[36]. The Vta1-Did2$_{176-204}$ complex buries a total of approximately 1039 Å^2 surface area at the interface, close to that (1115 Å^2) observed in the complex structure of Vps4-CHMP1A[20], but much larger than that (~624 Å^2) observed in the complex structures of LIP5NTD-CHMP1B and LIP5NTD-CHMP1B-CHMP5[36].

The interface in Vta1-Did2$_{176-204}$ complex structure. Two major kinds of interactions between Vta1NTD MIT1 domain and Did2$_{176-204}$ were observed (Fig. 3). One is predominantly hydrophobic, and is lined by the conserved and non-conserved residues Y25, L29, V32 and L36 in the 2nd helix, and residues A49, L53, I56 and F59 in the 3rd helix of Vta1NTD MIT1 (Fig. 3A and B). The side chains of the residues located at Did2$_{176-204}$ helix α6′, including L195′, A196′, L199′ and L202′, are inserted into the groove of Vta1NTD helices 2/3. Did2$_{176-204}$ L195′ side-chain has hydrophobic interaction with Vta1NTD A49, L53 and T46 side-chains, as residue L188 works in complex LIP5NTD-CHMP1B and LIP5NTD-CHMP1B-CHMP5 (Fig. 3D)[36], and residue L187 functions in complex Vps4A-CHMP1A MIM1 (Fig. 3E)[20]. Did2$_{176-204}$ A196′ has hydrophobic interactions with residue L36 of Vta1NTD (the distance is 2.3 Å between their methyl groups). Did2$_{176-204}$ L199′ side-chain methyl group has hydrophobic interactions with Vta1NTD L29 and V32 methyl groups (the distances between them are 2.3 Å), corresponding to residue L191 functioning in complex Vps4A-CHMP1A MIM1[20], and residue L192 working in complexes LIP5NTD-CHMP1B and LIP5NTD-CHMP1B-CHMP5[36]. In addition, Did2$_{176-204}$ L202′ side-chain also has hydrophobic interaction with Vta1NTD Y25, L29, V32, L53, I56, F59 and the side-chain of K60, similar to the observation of the residue L194 in complex Vps4A-CHMP1A MIM1[20], and residue L195 in complex LIP5NTD-CHMP1B and LIP5NTD-CHMP1B-CHMP5[36]. Besides these hydrophobic interactions, complementary salt bridges are further formed by two of the adjacent conserved Did2$_{176-204}$ residues (R198′and R203′) (Fig. 3C). Did2$_{176-204}$ R198′ forms a salt bridge with residues D54 and E57 in the 3rd helix of Vta1NTD, while Did2$_{176-204}$ R203′ has static electric interactions with negative side-chain of E33 in the 2nd helix of Vta1NTD. These interactions were also observed in the complex structure of LIP5NTD-CHMP1B
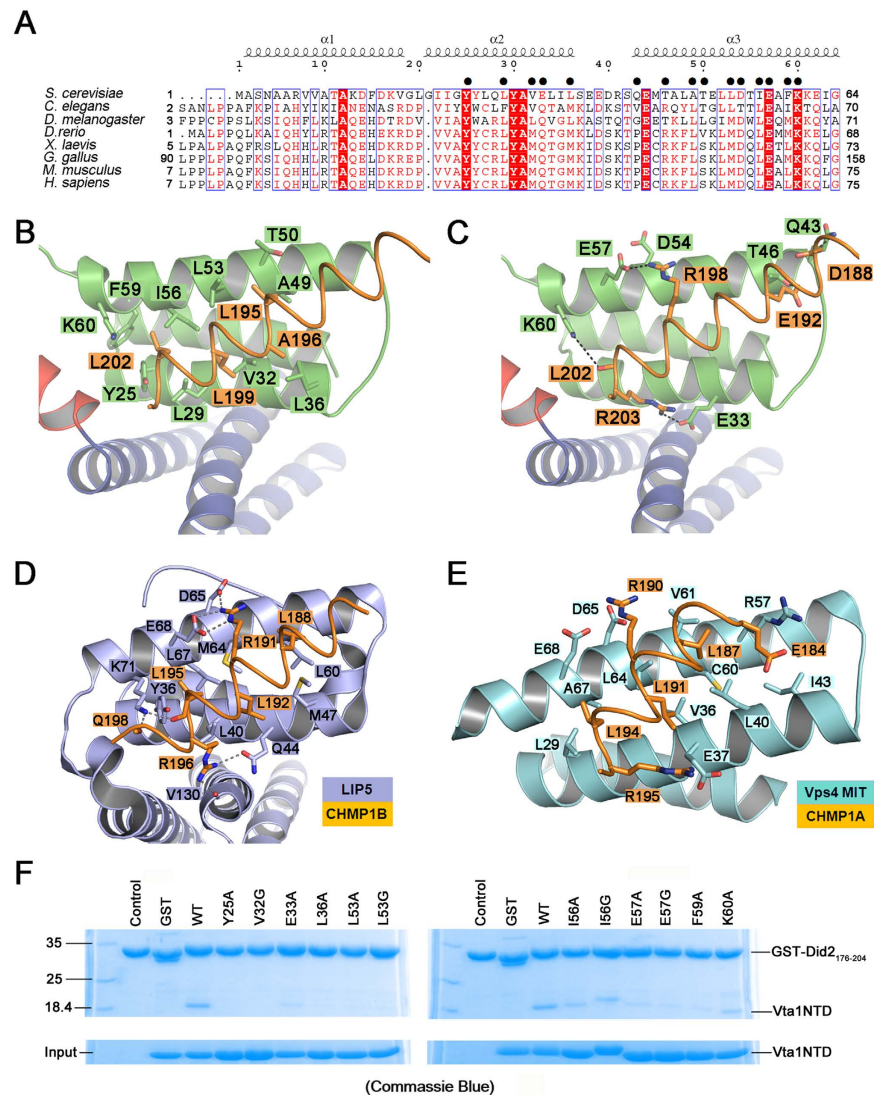
Figure 3. The conserved residues of Vta1NTD MIT1 domain interact with Did2₁₇₆₋₂₀₄. (**A**) Structure-based sequence alignment of Vta1NTD MIT1 from different organisms. The secondary structures of Vta1NTD MIT1 were displayed on the top of the sequences. The residues in MIT1 involved in the interaction between Vta1NTD and Did2₁₇₆₋₂₀₄ were marked by black dots. (**B,C**) The hydrophobic and electrostatic interactions observed in Vta1NTD-Did2₁₇₆₋₂₀₄ complex, where Vta1NTD is displayed in green cartoon, while Did2 is in orange ribbon mode, respectively. (**D,E**) Hydrophobic and electrostatic interactions observed in LIP5NTD-CHMP1B complex (pdb code 4TXQ), and in Vps4-CHMP1A complex (pdb code 2JQ9), respectively. CHMP1B and CHMP1A were displayed in orange, LIP5NTD MIT1 and Vps4 MIT1 were displayed in grey-blue, respectively. All residues involved in the interaction were highlighted in stick. (**F**) GST pull-down assay of the Vta1NTD-Did2₁₇₆₋₂₀₄ complex. GST or GST-tagged Did2₁₇₆₋₂₀₄ was used to pull down wild type or mutant Vta1NTD as indicated. Proteins retained on the beads were analyzed by SDS-PAGE and visualized by coomassie-blue staining. The control GST-tagged Did2₁₇₆₋₂₀₄ lane and the GST lane represented the cases where the gels were run in the absence of WT Vta1NTD. These two gels were run at different time.

and LIP5NTD-CHMP1B-CHMP5, corresponding to electric interaction between R191′ in CHMP1B and E68 in LIP5NTD, and hydrogen interaction between R196′ in CHMP1B and Q44 in LIP5NTD[36]. These two major type of interactions were also confirmed by our ITC experiment, with negative ΔH (−2.7 Kcal mol⁻¹) which can be attributed to the hydrogen-bond interaction as well as ionic interactions, and with positive ΔS (13.1 cal mol⁻¹ deg⁻¹) mainly derived from hydrophobic interactions in this case.

Mutations were introduced to these observed binding sites to test the importance of the residues to the overall stability of the complex. As shown in Fig. 3F, *in vitro* GST pull-down experiments demonstrate that all the single alanine or glycine substitutions of Vta1NTD residues Y25, E33, L36, L53, I56, E57, F59 and K60 have obvious effects on the Did2₁₇₆₋₂₀₄ binding, confirming the energetic importance of all those residues. Consistent with the relatively small buried interface area of Vta1NTD-Did2 complex (compared to the surface area at the interface of
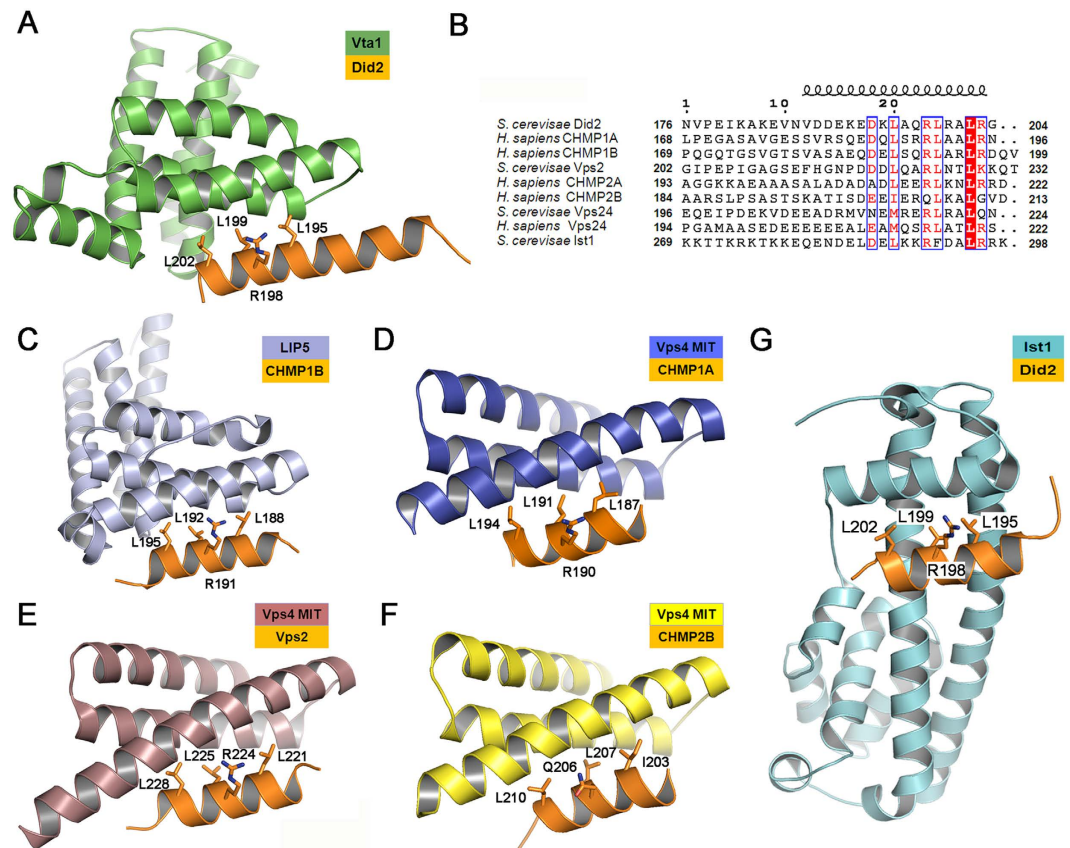
Figure 4. The conserved residues of Did2$_{176-204}$ interact with Vta1NTD in MIM1 mode. (**A**) Ribbon representation of Vta1NTD-Did2$_{176-204}$ complex. (**B**) Sequence alignments of Did2$_{176-204}$ containing helix α6′ with conserved MIM1 motif from various organisms. The helix conformation was displayed on the top of the sequences based on free Did2$_{176-204}$ structural calculation. (**C–F**) Ribbon representations of LIP5-CHMP1B complex (pdb code 4TXQ), Vps4 MIT-CHMP1A MIM1 complex (pdb code 2JQ9), Vps4 MIT-Vps2 MIM1 complex (pdb code 2V6X), and Vps4B MIT-CHMP2B complex (pdb code 2JQK); (**G**) Ribbon representation of Ist1NTD-Did2 complex (pdb code 3GGZ); In (**A,C–G**), all MIM1 domains were displayed in orange cartoon mode, and the conserved residues involved in the interactions were displayed in stick mode.

Vta1NTD-Vps60$_{128-186}$, approximately 3608 Å^2), each single site mutation dramatically decreases all Did2$_{176-204}$ binding, so that the binding affinities of all Vta1NTD variants to Did2$_{176-204}$ were non-detectable.

Did2 interacts with Vta1NTD in a classic MIM1 mode. The MIT domain is a versatile protein-protein interaction domain identified in proteins that have a role in vesicle trafficking, including Vps4, Vta1, AMSH and UBPY, where they mediate interaction within the ESCRT-III complex[41]. The MIT domain recognizes sequence motifs called the MIMs primarily within the ESCRT-III subunits. It has been implicated that the interaction between MIT and MIM acts in regulating the disassembly of ESCRT-III as well as targeting specific proteins to the site of ESCRT functions. As we summarized in previous report[33], five types of MIM (MIM1, MIM2, MIM3, MIM4 and MIM5) in total were reported to bind to different sites on the MIT domain[19–24]. Among them, MIM1 motif includes a sequence-conserved amphipathic helix (D/E)xxLxxRLxxL(K/R) along the groove between MIT helices α2 and α3 observed in the complexes Vps4-Vps2$_{183-232}$[19], Vps4-CHMP2B[19,20], LIP5-CHMP1B[36] and Vps4-CHMP1A$_{180-196}$[20] (Fig. 4A–F). MIM2 motif is a proline-rich sequence L$_{170}$P(E/D)VP$_{174}$ and R$_{183}$xLxPxLPxPP$_{193}$ along the groove between MIT helices α1 and α3 found in complex Vps4-CHMP6$_{168-179}$[21] and Saci1372-Saci1337$_{183-193}$[22], respectively. MIM3 motif is a highly specific mode along the groove between MIT helices α1 and α3 found in complex Spastin MIT-CHMP1B$_{148-196}$[23], but with a twice interface as large as that of MIT of the Vps4-CHMP complex. MIM4 motif is a mainly polar sequence E$_{203}$xxxExxφxxφxxRLx-TLR$_{221}$ along a groove made up by helices 3 (Vps4 MIT helix 2) and 4/5 (Vps4 MIT helix 3) identified in complex AMSHΔC-CHMP3ΔN[24]. MIM5 was found in Vta1NTD-Vps60 or LIP5NTD-CHMP5 complex[33,35]. Vps60 or CHMP5 MIM5 sequence (residues 140–186) forms two helices (α4′ and α5′), and binds two surfaces made up by helices 5, 7 (Vps4 MIT helices 1, 3) and helices 6, 7 (Vps4 MIT helices 2, 3) of the Vta1/LIP5 MIT2 domain. The Vta1/LIP5 MIT2-Vps60/CHMP5 MIM5 contacts are a mixture of polar and hydrophobic interactions as the same as the case of Spastin MIT-MIM3.

On one hand, Vta1NTD MIT1 derived from *S. cerevisiae* has a little higher sequence similarity with the other organisms than the Did2$_{176-204}$ sequence, as shown in Figs 3A and 4B. The conserved and non-conserved

hydrophobic residues L29, V32, L36, L53 and I56 (which present an overall hydrophobic surface), and hydrophilic residues E33, T46, D54, E57 and K60 in Vta1NTD MIT1 play more important roles in the Vta1-Did2 interactions. These residues correspond to the residues Y34, L37, M41, L64, A67, D38, R57, E68 and K71 in Vps4 MIT domain, all of which are involved in its interactions with CHMP1A MIM1 (Fig. 4E). On the other hand, in Vta1NTD-Did2$_{176-204}$ complex structure, the MIM region utilizes conserved hydrophobic residues L195′, L199′, and L202′ and hydrophilic residues R198′, R203′ to interact with MIT. These residues within Did2$_{176-204}$ helix α6′ in the interface make up of an amino acid sequence as E$_{192}$′xxL$_{195}$′xxR$_{198}$′L$_{199}$′xxL$_{202}$′R$_{203}$′, nearly identical to CHMP1A$_{180-196}$ MIM1 motif (D/E)xxLxxRLxxL(K/R)[19,20]. Thus, Did2 interacts with Vta1NTD through a classic MIM1 mode. Interestingly, although the binding mode of Did2 and Vta1NTD resembles that of LIP5NTD-CHMP1B, the extent of their further stimulation for Vps4 activity diverge from each other, which suggests different mechanism for Did2 or CHMP1B involved in MVB pathway.

In addition, as shown in Fig. 4G, the crystal structure of Ist1NTD-Did2 MIM1 complex indicated that Did2 MIM1 interacts with the groove made up by Ist1NTD helices α1, α3 and α5 through hydrophobic residues L195′, L199′, L202′ and positively charged residues R198′ and R203′ in helix α6′[42]. This observation suggested that Did2 MIM1 could not simultaneously interact with Vta1NTD and Ist1NTD. Moreover, the binding affinity (K_D) of Ist1 to Did2 MIM1 is close to 1 μM, much stronger than that ($K_D = \sim 39$ μM) of Vps4 MIT domain binding to Did2 MIM1, and that ($K_D = \sim 28$ μM) Vps4 MIT domain binding to Vps2 MIM1 domain, and that ($K_D = 12.8$ μM) of Vta1NTD binding to Did2 MIM1. This observation reveals that Did2 MIM1 may prefer bind to Ist1NTD due to stronger binding affinity than that to Vta1NTD, and that the interaction between MIT and MIM1 domains in ESCRT-III system is not significantly specific. This analysis may interpret why MIT domain can interact with different subunits in ESCRT-III containing MIM1 domain.

Either Did2 or Vps60 enhances Vta1 stimulation of Vps4 in a specifically indirect manner.
The dynamic assembly and disassembly of the ESCRT-III polymer play a critical role in ESCRT-mediated membrane deformation events, and the alterations of Vps4 ATPase activity. To address how Vps60 and Did2 binding enhance Vta1 stimulation of Vps4 ATPase activity, two models were previously presented[27]. One is that their binding to MIT domains results in the conformation changes of Vta1; the other is that the interaction between Vta1 and Did2 or Vps60 increases the local concentration of Vta1–Vps4 in vitro. It was reported that removal of the two Vta1 tandem MIT domains (Vta1$_{165-330}$) does not enhance the basal activation of Vps4 by Vta1, implying that Vta1 MIT domains does not autoinhibit Vps4 activation[27]. The NMR structures of complex Vta1NTD-Vps60$_{128-186}$[33–35] and Vta1NTD-Did2$_{176-204}$ provided evidences that the Vps60 or Did2-binding did not induce overall conformational changes in the N-terminus of Vta1. These observations suggested that either Did2 or Vps60 did not allosterically regulate Vta1NTD and thus could not potentiate its ability to directly activate Vps4. Recently, at C-terminus of Vta1, a novel short amino acid sequence, called as Vps4 stimulatory element (VSE), was identified to be released to stimulate Vps4 ATPase activities, upon Vta1NTD interacting with ESCRT-III Did2 or Vps60[43]. VSE activity is auto-inhibited in a manner dependent upon the unstructured linker region, which joints the N-terminal MIT domains and the C-terminal VSL domain. Thus, although structural studies on Vta1NTD-Vps60$_{128-186}$ and Vta1NTD-Did2$_{176-204}$ provided no direct evidences of how Vps60 and Did2 function, Vps60 or Did2 binding to Vta1NTD might lead to further structural arrangement in the C-terminal domain of Vta1. Either Did2 or Vps60 enhances Vta1 stimulation of Vps4 in a specifically indirect manner.

In summary, we determined NMR solution structure of Vta1NTD-Did2$_{176-204}$, which provided the molecular basis of how Did2 interacts with Vta1NTD. Structural comparison and sequence alignment suggest that Did2 binds to Vta1NTD in a classic MIM1 mode. Both Vps60$_{128-186}$ and Did2$_{176-204}$ stimulate Vps4 activities by releasing VSE through interaction with Vta1NTD.

Methods

Cloning, expression, and purification.
DNA fragments encoding yeast Vta1 and Did2 were amplified from the *S. cerevisiae* genomic DNA. Vta1NTD and Did2$_{176-204}$ were expressed in *Escherichia coli* BL21(DE3) using a modified pET28b vector with a SUMO protein inserted between a His$_6$-tag and the Vta1NTD or Did2$_{176-204}$ coding region, respectively. To correctly estimate the concentration of Did2$_{176-204}$ during its purification, an extra residue tryptophan was inserted in the N-terminus of the peptide during constructing the plasmid. To obtain pure Vta1NTD, the His$_6$-tagged SUMO-Vta1NTD was purified by Ni^{2+}-NTA affinity chromatography (GE Healthcare, USA) following standard procedures. ULP1 protease was then added to remove the His$_6$-SUMO tag and the protein mixture was passed over a second Ni^{2+}-NTA column and was further purified by anion exchange chromatography on a Resource Q column (GE Healthcare, USA). The Vta1NTD variants were purified in the same way as native proteins. To prepare pure Did2$_{176-204}$, the His$_6$-tagged SUMO Did2$_{176-204}$ was first purified by Ni^{2+}-NTA affinity chromatography and by anion exchange chromatography on a Resource Q column, respectively. Then ULP1 protease was added to remove the His$_6$-SUMO tag, and the protein mixture was passed over a gel-filtration chromatography Superdex 75 column (GE Healthcare, USA). The concentration of Did2$_{176-204}$ was finally obtained from the absorbance at 280 nm with an absorption coefficient of 5500 M^{-1}cm^{-1}. The peptide solution was lyophilized for future usage.

For isotope labeling NMR sample (either Vta1NTD or Did2$_{176-204}$), M9 minimal medium was used supplemented with ^{15}NH$_4$Cl (Cambridge Isotope Laboratories, USA) or ^{15}NH$_4$Cl and ^{13}C-glucose (Cambridge Isotope Laboratories, USA), or ^{15}NH$_4$Cl, ^{13}C-glucose and 70% D$_2$O (Cambridge Isotope Laboratories, USA).

NMR sample preparation and data collection.
Differentially labeled complex samples in NMR buffer (25 mM sodium phosphate pH 7.0, 100 mM NaCl, 5 mM dithiothreitol-d$_{10}$ (DTT), 0.02% NaN$_3$, 10% D$_2$O), were prepared as follows: 1) 1.5 mM uniformly ^{15}N-/^{13}C double labeled or ^{15}N-/^{13}C-/70% ^{2}H triple labeled Vta1NTD plus 1.8 mM unlabeled Did2$_{176-204}$; 2) 1.5 mM uniformly labeled ^{15}N-/^{13}C-labeled Did2$_{176-204}$ in

complex with 1.8 mM unlabeled Vta1NTD. All NMR experiments were performed at 20 °C on a Varian Unity Inova 600 NMR spectrometer (with cryo-probe) equipped with triple resonances and pulsed field gradients, or on a Bruker Avance III-800 MHz NMR spectrometer (with cryo-probe) equipped with four channels and z-axis pulsed-field gradient. The standard suite of experiments for assigning the ^{1}H, ^{13}C and ^{15}N backbone and side chain chemical shifts of ^{13}C and ^{15}N double labeled Vta1NTD in complex with unlabeled Did2$_{176-204}$, or of ^{13}C and ^{15}N double labeled Did2$_{176-204}$ in complex with unlabeled Vta1NTD, and for the collection of NOE-based distance restraints were measured[44,45], including the two-dimensional (2D) ^{13}C-edited HSQC in both aliphatic and aromatic regions, and ^{15}N-edited HSQC; the three-dimensional (3D) HNCA, HNCO, HN(CO)CA, HNCACB, CBCA(CO)NH, ^{15}N-resolved HSQC-TOCSY, HCCH-TOCSY in both aliphatic and aromatic regions, ^{15}N-resolved HSQC-NOESY, ^{13}C-resolved HSQC-NOESY for both aliphatic and aromatic resonances, 2D (H$_\beta$) C$_\beta$(C$_\gamma$C$_\delta$)H$_\delta$ and (H$_\beta$)C$_\beta$(C$_\gamma$C$_\delta$C$_\epsilon$)H$_\epsilon$ spectra for correlation of C$_\beta$ and H$_\delta$ or H$_\epsilon$ in aromatic ring used in aromatic protons assignment[46]. The intermolecular NOEs between isotope labeled Vta1NTD or Did2$_{176-204}$ peptide and unlabeled Did2$_{176-204}$ peptide or Vta1NTD were obtained by analyzing 3D ^{13}C-F1 edited, ^{13}C/^{15}N-F3 filtered NOESY spectra, respectively.

For assignment of NMR signals belonging to free Did2$_{176-204}$, the isotope ^{15}N-labeled Did2$_{176-204}$ and unlabeled Did2$_{176-204}$ were used at the concentration of 1.0 mM in NMR buffer. 2D ^{1}H-^{1}H TOCSY and NOESY, as well as 3D ^{15}N-edited HSQC-TOCSY experiment, were acquired at 20 °C only on the Varian Unity Inova 600 NMR spectrometer (with cryo-probe, as mentioned above).

All spectra were processed with the program NMRPipe[39] and analyzed with the Sparky 3 software[47]. The ^{1}H chemical shifts were referenced to 2,2-dimethylsilapentane-5-sulfonic acid (DSS), and the ^{13}C- and ^{15}N-resonances were indirectly referenced DSS.

NMR structure determination. The structural calculations of free Did2$_{176-204}$ and of the complex Vta1NTD-Did2$_{176-204}$ were carried out using a standard simulated annealing protocol implemented in the program XPLOR-2.19 (NIH version). The inter-proton distance restraints derived from NOE intensities were grouped into three distance ranges 1.8–2.9 Å, 1.8–3.5 Å and 1.8–6.0 Å, corresponding to strong, medium and weak NOEs, respectively. The dihedral angles phi and psi were derived from the backbone chemical shifts (HN, HA, CO, CA) by the program TALOS[39,40]. Slowly exchanging amide protons, identified in the 2D ^{15}N-HSQC spectra recorded after a H$_2$O buffer was exchanged to a D$_2$O buffer, were used in the structure calculated with the NOE distances restraints to generate hydrogen bonds for the final structure calculation, as done in the literature[48]. A total of ten iterations[49] structures in the initial eight iterations were performed. 100 structures were computed in the last two iterations, 20 conformers with the lowest energy are used to represent the 3D structures. In the ensemble of the simulated annealing 20 structures, there was no distance constraint violation more than 0.3 Å and no torsion angle violation more than 3°. The final 20 structures of the complex Vta1NTD-Did2$_{176-204}$ or free Did2$_{176-204}$ with lowest energy were evaluated with the program PROCHECK-NMR and PROCHECK[50] and summarized in Table 1. All figures were generated using the program PyMOL (http://pymol.org/) and MOLMOL[49].

Isothermal titration calorimetry (ITC) assay. To obtain a direct binding affinity between Vta1NTD and Did2$_{176-204}$ peptide, solution of about 0.1 mM Vta1NTD was titrated with 2.0 mM Did2$_{176-204}$ peptide using iTC-200 microcalorimeter (GE healthcare, USA) at 25 °C. The protein and peptide were exchanged to a buffer containing 25 mM sodium phosphate, pH 7.0 and 50 mM NaCl by gel-filtration chromatography, centrifuged to remove any particulates, and degassed. The accurate concentrations of Vta1NTD and Did2$_{176-204}$ concentration were determined using their A^{280} coefficient constants. The obtained data were fitted by a nonlinear least squares approach to the 'one set of sites' binding model from Microcal Origin software, which yielded the association constant (K_a), stoichiometry of binding (n), and the thermodynamic parameters, enthalpy change of binding (ΔH), entropy change of binding (ΔS) and free energy change of binding (ΔG). The ITC experiment was repeated at least two times for validity.

GST pull-down experiments. The experiments were performed following standard procedures in buffer containing 25 mM Tris-HCl (pH 8.0), 150 mM NaCl, and 5 mM 2-mercaptoethanol. Purified WT Vta1NTD and its mutants were incubated with either GST alone or GST-tagged Did2$_{176-204}$ immobilized on glutathione agarose beads for 3 h at 4 °C. The beads were then washed extensively with above buffer three times, and bound proteins were separated on SDS-PAGE and visualized by Coomassie-blue staining. The pull-down experiments were repeated three times with the similar results. The representative results were shown in Fig. 3F. The control GST-tagged Did2$_{176-204}$ alone lane and the GST alone lane indicated the cases where the gels were run in the absence of WT Vta1NTD. The two gels were run at different time.

References

1. Babst, M. A protein's final ESCRT. *Traffic* **6**, 2–9 (2005).
2. Hurley, J. H. & Emr, S. D. The ESCRT complexes: structure and mechanism of a membrane-trafficking network. *Annu Rev Biophys Biomol Struct* **35**, 277–298 (2006).
3. Piper, R. C. & Katzmann, D. J. Biogenesis and function of multivesicular bodies. *Annu Rev Cell Dev Biol* **23**, 519–547 (2007).
4. Winter, V. & Hauser, M. T. Exploring the ESCRTing machinery in eukaryotes. *Trends Plant Sci* **11**, 115–123 (2006).
5. Gruenberg, J. & Stenmark, H. The biogenesis of multivesicular endosomes. *Nat Rev Mol Cell Biol* **5**, 317–323 (2004).
6. Morita, E. & Sundquist, W. I. Retrovirus budding. *Annu Rev Cell Dev Biol* **20**, 395–425 (2004).
7. Carlton, J. G. & Martin-Serrano, J. Parallels between cytokinesis and retroviral budding: a role for the ESCRT machinery. *Science* **316**, 1908–1912 (2007).
8. Saksena, S. & Emr, S. D. ESCRTs and human disease. *Biochem Soc Trans* **37**, 167–172 (2009).
9. Raiborg, C. & Stenmark, H. The ESCRT machinery in endosomal sorting of ubiquitylated membrane proteins. *Nature* **458**, 445–452 (2009).

10. Bieniasz, P. D. The cell biology of HIV-1 virion genesis. *Cell Host Microbe* **5,** 550–558 (2009).
11. Fujii, K., Hurley, J. H. & Freed, E. O. Beyond Tsg101: the role of Alix in 'ESCRTing' HIV-1. *Nat Rev Microbiol* **5,** 912–916 (2007).
12. Williams, R. L. & Urbe, S. The emerging shape of the ESCRT machinery. *Nat Rev Mol Cell Biol* **8,** 355–368 (2007).
13. Hurley, J. H. ESCRT complexes and the biogenesis of multivesicular bodies. *Curr Opin Cell Biology* **20,** 4–11 (2008).
14. Babst, M., Wendland, B., Estepa, E. J. & Emr, S. D. The Vps4p AAA ATPase regulates membrane association of a Vps protein complex required for normal endosome function. *EMBO J* **17,** 2982–2993 (1998).
15. Xiao, J., Xia, H., Yoshino-Koh, K., Zhou, J. & Xu, Z. Structural characterization of the ATPase reaction cycle of endosomal AAA protein Vps4. *J Mol Biol* **374,** 655–670 (2007).
16. Katzmann, D. J., Odorizzi, G. & Emr, S. D. Receptor downregulation and multivesicular-body sorting. *Nat Rev Mol Cell Biol* **3,** 893–905 (2002).
17. Yu, Z., Gonciarz, M. D., Sundquist, W. I., Hill, C. P. & Jensen, G. J. Cryo-EM structure of dodecameric Vps4p and its 2:1 complex with Vta1p. *J Mol Biol* **377,** 364–377 (2008).
18. Shestakova, A. *et al.* Assembly of the AAA ATPase Vps4 on ESCRT-III. *Mol Biol Cell* **21,** 1059–1071 (2010).
19. Obita, T. *et al.* Structural basis for selective recognition of ESCRT-III by the AAA ATPase Vps4. *Nature* **449,** 735–711 (2007).
20. Stuchell-Brereton, M. D. *et al.* ESCRT-III recognition by VPS4 ATPases. *Nature* **449,** 740–744 (2007).
21. Kieffer, C. *et al.* Two distinct modes of ESCRT-III recognition are required for VPS4 functions in lysosomal protein targeting and HIV-1 budding. *Dev Cell* **15,** 62–73 (2008).
22. Samson, R. Y., Obita, T., Freund, S. M., Williams, R. L. & Bell, S. D. A role for the ESCRT system in cell division in archaea. *Science* **322,** 1710–1713 (2008).
23. Yang, D. *et al.* Structural basis for midbody targeting of spastin by the ESCRT-III protein CHMP1B. *Nat Struct Mol Biol* **15,** 1278–1286 (2008).
24. Solomons, J. *et al.* Structural basis for ESCRT-III CHMP3 recruitment of AMSH. *Structure* **19,** 1149–1159 (2011).
25. Babst, M., Davies, B. A. & Katzmann, D. J. Regulation of Vps4 during MVB sorting and cytokinesis. *Traffic* **12,** 1298–1305 (2011).
26. Azmi, I. *et al.* Recycling of ESCRTs by the AAA-ATPase Vps4 is regulated by a conserved VSL region in Vta1. *J Cell Biol* **172,** 705–717 (2006).
27. Azmi, I. F. *et al.* ESCRT-III family members stimulate Vps4 ATPase activity directly or via Vta1. *Dev Cell* **14,** 50–61 (2008).
28. Dimaano, C., Jones, C. B., Hanono, A., Curtiss, M. & Babst, M. Ist1 regulates Vps4 localization and assembly. *Mol Biol Cell* **19,** 465–474 (2008).
29. Xiao, J. *et al.* Structural basis of Vta1 function in the multivesicular body sorting pathway. *Dev Cell* **14,** 37–49 (2008).
30. Lottridge, J. M., Flannery, A. R., Vincelli, J. L. & Stevens, T. H. Vta1p and Vps46p regulate the membrane association and ATPase activity of Vps4p at the yeast multivesicular body. *Proc Natl Acad Sci USA* **103,** 6202–6207 (2006).
31. Scott, A. *et al.* Structural and mechanistic studies of VPS4 proteins. *EMBO J* **24,** 3658–3669 (2005).
32. Yang, D. & Hurley, J. H. Structural role of the Vps4-Vta1 interface in ESCRT-III recycling. *Structure* **18,** 976–984 (2010).
33. Yang, Z. *et al.* Structural basis of molecular recognition between ESCRT-III-like protein Vps60 and AAA-ATPase regulator Vta1 in the multivesicular body pathway. *J Biol Chem*. **287,** 43899–43908 (2012).
34. Yang, Z. *et al.* ¹H, ¹³C and ¹⁵N resonance assignments of the N-terminal domain of Vta1-Vps60 peptide complex. *Biomol NMR Assign* **7,** 331–334 (2013).
35. Skalicky, J. J. *et al.* Interactions of the human LIP5 regulatory protein with endosomal sorting complexes required for transport. *J Biol Chem* **287,** 43910–43926 (2012).
36. Vild, C. J., Li, Y., Guo, E. Z., Liu, Y. & Xu, Z. A Novel Mechanism of Regulating the ATPase VPS4 by Its Cofactor LIP5 and the Endosomal Sorting Complex Required for Transport (ESCRT)-III Protein CHMP5. *J Biol Chem* **290,** 7291–7303 (2015).
37. Muziol, T. *et al.* Structural basis for budding by the ESCRT-III factor CHMP3. *Dev Cell* **10,** 821–830 (2006).
38. Wishart, D. S. & Sykes, B. D. The ¹³C chemical-shift index: a simple method for the identification of protein secondary structure using 13C chemical-shift data. *J Biomol Nmr* **4,** 171–180 (1994).
39. Delaglio, F. *et al.* NMRPipe: a multidimensional spectral processing system based on UNIX pipes. *J Biomol Nmr* **6,** 277–293 (1995).
40. Cornilescu, G., Delaglio, F. & Bax, A. Protein backbone angle restraints from searching a database for chemical shift and sequence homology. *J Biomol Nmr* **13,** 289–302 (1999).
41. Hurley, J. H. & Yang, D. MIT domainia. *Dev Cell* **14,** 6–8 (2008).
42. Xiao, J. *et al.* Structural basis of Ist1 function and Ist1-Did2 interaction in the multivesicular body pathway and cytokinesis. *Mol Biol Cell* **20,** 3514–3524 (2009).
43. Shestakova, A., Curtiss, M., Davies, B. A., Katzmann, D. J. & Babst, M. The linker region plays a regulatory role in assembly and activity of the Vps4 AAA ATPase. *J Biol Chem* **288,** 26810–26819 (2013).
44. Bax, A. & Grzesiek, S. Methodological Advances in Protein Nmr. *Accounts Chem Res* **26,** 131–138 (1993).
45. Clore, G. M. & Gronenborn, A. M. Determining the structures of large proteins and protein complexes by NMR. *Trends Biotechnol* **16,** 22–34 (1998).
46. Yamazaki, T., Formankay, J. D. & Kay, L. E. 2-Dimensional Nmr Experiments for Correlating C-13-Beta and H-1-Delta/Epsilon Chemical-Shifts of Aromatic Residues in C-13-Labeled Proteins Via Scalar Couplings. *J Am Chem Soc* **115,** 11054–11055 (1993).
47. Goddard, T. D. & Kneller, D. G. *SPARKY 3.* (University of California, San Francisco) (2001).
48. Wang, C. *et al.* Structural basis for site-specific reading of unmodified R2 of histone H3 tail by UHRF1 PHD finger. *Cell Res* **21,** 1379–1382 (2011).
49. Koradi, R., Billeter, M. & Wuthrich, K. MOLMOL: a program for display and analysis of macromolecular structures. *J Mol Graph* **14,** 51–55 29–32 (1996).
50. Laskowski, R. A., Rullmann, J. A., MacArthur, M. W., Kaptein, R. & Thornton, J. M. AQUA and PROCHECK-NMR: programs for checking the quality of protein structures solved by NMR. *J Biomol Nmr* **8,** 477–486 (1996).

Acknowledgements

Author Contributions

C.C. Z.X. conceived and designed the experiments, C.C. wrote the manuscript; C.J.W. made the plasmid of Vta1NTD. J.S. and Z.Y. performed protein preparation, NMR experiments in 600 MHz, NMR assignments and structural calculation. J.W. did mutation studies. X.Z. and M.L. did NMR experiments in 800 MHz, B.Z., W.L., C.W. analyzed the data and helped writing manuscript. All authors reviewed the manuscript.

Additional Information

Competing financial interests: The authors declare no competing financial interests.

How to cite this article: Shen, J. *et al.* NMR studies on the interactions between yeast Vta1 and Did2 during the multivesicular bodies sorting pathway. *Sci. Rep.* **6**, 38710; doi: 10.1038/srep38710 (2016).

Publisher's note: Springer Nature remains neutral with regard to jurisdictional claims in published maps and institutional affiliations.